DOI: 10.37190/abb/220943

Design and Analysis of Rehabilitation Training Mechanism Based on Upper Limb Rehabilitation Movements

Haoyu Han[1], Qinghui Zhu[1], Li Feng[1*]

[1]College of Home and Art Design, Northeast Forestry University, Harbin, Heilongjiang, 150000, China

[*]Corresponding author: Li Feng, College of Home and Art Design, Northeast Forestry University, Harbin, Heilongjiang, 150000, China, e-mail address: fengli86@nefu.edu.cn

Submitted: 10th March 2026

Accepted: 21st April 2026

ACCEPTED

Abstract:

Purpose: To conduct a comparative analysis of the trajectory and joint torque differences between exoskeleton type and end-effector type upper limb rehabilitation training mechanisms during rehabilitation movements, and to identify the more suitable mechanism type for passive upper limb rehabilitation training.

Methods: Based on the Brunnstrom rehabilitation approach, upper limb rehabilitation movements for the passive training phase were selected. Muscle force simulations were conducted using OpenSim software to identify movements with high muscular engagement. The structures of the two mechanisms were designed through degree-of-freedom analysis, and motion trajectory simulations were completed in ADAMS. In MATLAB, discrete Fréchet distance is used to evaluate trajectory similarity. Calculate the error of comparing the trajectories of two mechanisms with the trajectory of the human body model at the same time using R^2. In ADAMS, compare the rotational torque changes of the shoulder, elbow, and wrist joints between two mechanisms.

Results: The movement trajectory of the exoskeleton mechanism closely matched the natural motion of the human upper limb, error $\leq$ 2 mm, trajectory $R^2 \geq 0.9975$. Its joint torque distribution was balanced, with a maximum torque $\leq$ 40 Nm. The trajectory error of the end-effector mechanism $\leq$5 mm, trajectory $R^2 \geq 0.9910$ and torques were concentrated at the wrist and elbow joints, some values $\geq$ 40 Nm.

Conclusion: The exoskeleton-type upper limb rehabilitation training mechanism demonstrates superior performance in terms of movement trajectory adaptability and joint protection compared to the end-effector-type mechanism, making it more suitable for passive movement assistance and joint range of motion recovery training. for passive motion assistance and joint range of motion recovery training.

Keywords: Rehabilitation training; Rehabilitation device; Mechanism design; Trajectory fitting; Mechanism analysis

ACCEPTED

1. Introduction

Based on research data from the National Institutes of Health (NIH), there has been a significant expansion in the number of patients with upper limb dysfunction caused by stroke, with an annual global increase of ten million cases. The sharp rise in patient numbers has promoted the development of upper limb rehabilitation training institutions [4, 17]. Among these, upper limb rehabilitation trainers with rigid series mechanical structures have become a hot research topic in the field of rehabilitation medicine due to their advantages such as strong structural stability, high motion control precision, and good repeatability [14, 18].

Currently, upper limb rehabilitation devices based on rigid series mechanical structures are mainly divided into two types: end-effector type and exoskeleton wearable type [11]. The end-effector structure drives the upper limb movement through traction by securely connecting the actuator to the distal end of the human upper limb. The exoskeleton structure binds directly to the human upper limb, assisting joint movements and allowing precise control over each joint.

Research on end-effector mechanisms focuses on achieving safe, compliant, and functionally appropriate trajectory planning and tracking within complex human-robot interaction spaces. To prevent joint velocity surges at the terminal connection from injuring patients during extensive rehabilitation training, recent studies aim to correct mechanism trajectory deviations in rehabilitation scenarios. By establishing spatial tolerance constraints, impedance control, and other mechanisms, real-time management of the motion range of rehabilitation training devices is achieved, constructing an end-effector mechanism that aligns with upper limb rehabilitation movements [6, 19]. In terms of trajectory control, research on end-effector mechanisms primarily involves personalized trajectory customization and compliant tracking control. Studies have developed a system for personalized trajectory acquisition and optimization, preserving topological features through force compensation strategies and data compression techniques. Combining curve interpolation with improved optimization algorithms enhances trajectory smoothness, addressing the insufficient adaptability caused by

ACCEPTED

traditional generalized trajectories. A composite tracking control strategy integrating multiple algorithms was designed, combining adaptive control, feedforward control, and impedance-admittance switching mechanisms. This significantly improves human-robot interaction compliance and safety while ensuring trajectory tracking accuracy. Research demonstrates that such mechanisms, designed through trajectory planning, can effectively achieve personalized trajectory adaptation and high-precision compliant tracking [2, 3, 9]. Research on exoskeleton mechanisms centers on enhancing the naturalness of human-robot interaction and control intelligence. To overcome the inherent limitation of traditional rigid exoskeletons restricting natural movement due to mismatched joint axes, recent efforts focus on developing bionic joints and human motion simulation technologies. Through trajectory planning mapping the training process of human joint stiffness characteristics, exoskeleton mechanisms closely matching upper limb rehabilitation movements are constructed [8, 15]. In trajectory planning and control, core research areas for exoskeleton mechanisms include human-robot collaboration accuracy optimization, safety control system construction, and personalized collaborative trajectory planning. Mechanical structure design driven by anatomical features combined with kinematic modeling enables precise alignment between exoskeleton joint motions and physiological human joints, markedly improving human-robot compatibility in trajectory tracking. Compensatory abnormal motion detection is integrated into the closed-loop trajectory control system. Using multi-sensor fusion to collect force, displacement, and trajectory data, machine learning algorithms identify and suppress abnormal motions, effectively reducing risks of secondary injuries during rehabilitation training. Optimal trajectories are selected through alignment, motion pattern extraction, generalization generation algorithms, and patient engagement models, overcoming limitations of conventional unilateral training approaches. Studies validate that these mechanisms, designed with trajectory control strategies, substantially enhance trajectory tracking precision, human-robot synergy, and training safety [1, 5, 16]

In summary, in the research on upper limb rehabilitation trainers based on trajectory control, researchers continuously simulate trajectory planning to better align

ACCEPTED

with human motion. Currently, the design methods of upper limb rehabilitation devices using trajectory planning control have become very mature for both exoskeleton-type and end-effector-type structures. However, there is still limited research comparing the trajectory differences between these two types of upper limb rehabilitation devices under the same action trajectory changes, as well as analyzing the joint moments of various upper limb joints during movement. This makes it difficult to select an appropriate type of rehabilitation device when designing such equipment.

Therefore, to compare and analyze whether both types of upper limb rehabilitation devices can complete the designer's training tasks under specific actions and to identify their differences under the same action, this paper selects upper limb rehabilitation exercises from the passive training component of Brunnstrom rehabilitation technique. Using OpenSim software, we analyze changes in muscle force during upper limb rehabilitation movements and select those that highly engage upper limb muscles. Based on degrees of freedom analysis, we design upper limb rehabilitation trainers with exoskeleton-type and end-effector-type structures. We use ADAMS to simulate the motion trajectories of both mechanisms and employ discrete Fréchet distance in MATLAB to analyze the similarity between the trajectory curves of the two rehabilitation devices and actual rehabilitation exercises. Additionally, we analyze the joint driving moments of both rehabilitation devices under the same rehabilitation exercise trajectory, ultimately selecting a more suitable mechanism for rehabilitation training. Unlike previous studies that independently optimize either exoskeleton or end-effector systems, this study proposes a unified comparative framework under identical physiological trajectory constraints. By integrating musculoskeletal simulation, multibody dynamics, and trajectory similarity analysis, the study provides a quantitative cross-mechanism evaluation of both kinematic fidelity and joint torque distribution. This combined evaluation framework represents the primary methodological contribution of this work.

ACCEPTED

2. Materials and Methods

2.1 Selection and Kinematic Data Acquisition of Rehabilitation Movements

To establish a physiological baseline for the rehabilitation devices, passive upper limb exercises corresponding to the first stage (flaccid stage) of the Brunnstrom recovery approach were selected. Collect joint rotation angles of the shoulder and elbow joints in six movements (elbow flexion, horizontal adduction/abduction, vertical abduction/adduction, flexion/extension, shoulder internal/external rotation, elbow internal/external rotation) through joint range of motion measurement experiments. Elbow flexion refers to the flexion of the forearm in the sagittal plane, the horizontal adduction/abduction refers to the adduction/abduction of the upper limb in the horizontal plane, the vertical abduction/adduction refers to the abduction/adduction of the upper limb in the coronal plane, the flexion/extension refers to the extension of the upper limb in the sagittal plane, the shoulder internal/external rotation refers to the internal/external rotation of the shoulder joint in the sagittal plane, the elbow internal/external rotation joint refers to the internal/external rotation of the elbow joint in the sagittal plane. The experimental subjects were 10 adult volunteers (table 1), measured using a clinical goniometer and a standard range of motion (ROM) scale. Record the data of the shoulder and elbow joints in 5 measurement experiments and calculate the average ROM value (table 2). Movements with minimal or clinically insignificant rotational ranges in the coronal plane were excluded from subsequent biomechanical analyses to ensure the selected trajectories provided comprehensive muscle engagement.

Table 1 Volunteer information

Information	Max	Min	X±SD
Age(year)	35	20	26±3.2
Height(cm)	161	184	169.24±6.41
Weight(kg)	49	82	66.43±8.23

ACCEPTED

Table 2 Range of motion of joints

Rehabilitation movement	Shoulder coronal plane ROM	Shoulder sagittal plane ROM	Shoulder transverse plane ROM	Elbow coronal plane ROM	Elbow sagittal plane ROM	Elbow transverse plane ROM
Elbow flexion	0°	0°	0°	0°	0-91.5°	0°
Horizontal adduction/abduction	0°	0°	0-91.3°	0°	0°	0-93.5°
Vertical abduction/adduction	0°	-30.6-89.1°	0°	0°	0°	0°
Flexion/extension	0-92.1°	0°	0°	0°	0°	0°
Shoulder internal/external rotation	0°	0°	0°	0-62.4°	0°	0°
Elbow internal/external rotation	0°	0°	0°	0-29.5°	0°	0°

2.2 Biomechanical Simulation and Muscle Force Analysis

To objectively identify movements with the highest therapeutic efficacy (i.e., optimal muscle activation intensity), biomechanical simulations were conducted using OpenSim 4.3 software. Use the DAS3-version2.osim file provided on the OpenSim official website as the basic model for biomechanical simulation of the human upper limb musculoskeletal model. The DAS3 model is an improved version based on the Delft Shoulder and Elbow Model (DSEM) and specifically adapted for the OpenSim environment. The model was mainly developed by the biomechanics research group at Delft University of Technology in the Netherlands. Based on the DAS3 model technical documentation and related papers provided by the official platform [12, 13], summarize the basic information of the model (table 3) (fig. 1). The advantage of this model compared to the basic model provided in opensim is that DAS3 uses ellipsoidal constraints to simulate scapular sliding at the shoulder joint, which can ignore the deviation of the shoulder axis caused by scapular sliding when analyzing movements.

This paper uses joint movement angles as input data for upper limb muscle force simulation, can directly use the upper limb data included in the DAS3 model for

ACCEPTED

simulation analysis. Simulation workflow consisted of three primary stages. Firstly, convert the time-series joint angle data obtained from clinical measurements (table 2) into a .trc format file available in opensim and input it into the Inverse Kinematics (IK) tool to generate motion data files (.mot) for the selected movements, with the processed inverse kinematics data for the shoulder and elbow joints summarized (tables 4 and 5), respectively. Subsequently, the Inverse Dynamics (ID) analyzer was applied to compute the required joint moments. Finally, use a static optimization (SO) solver to calculate the dynamic changes in muscle strength of the upper arm and forearm muscle groups throughout the entire rehabilitation cycle, and analyze the biomechanical potential of the upper arm muscle groups being stretched and involved. It should be noted that using static optimization for muscle force estimation does not necessarily mean that muscles will actively contribute during passive rehabilitation. This article uses hypothetical active motion simulation to select the action that stimulates the upper limb muscle group the most, as the target trajectory for passive rehabilitation training.

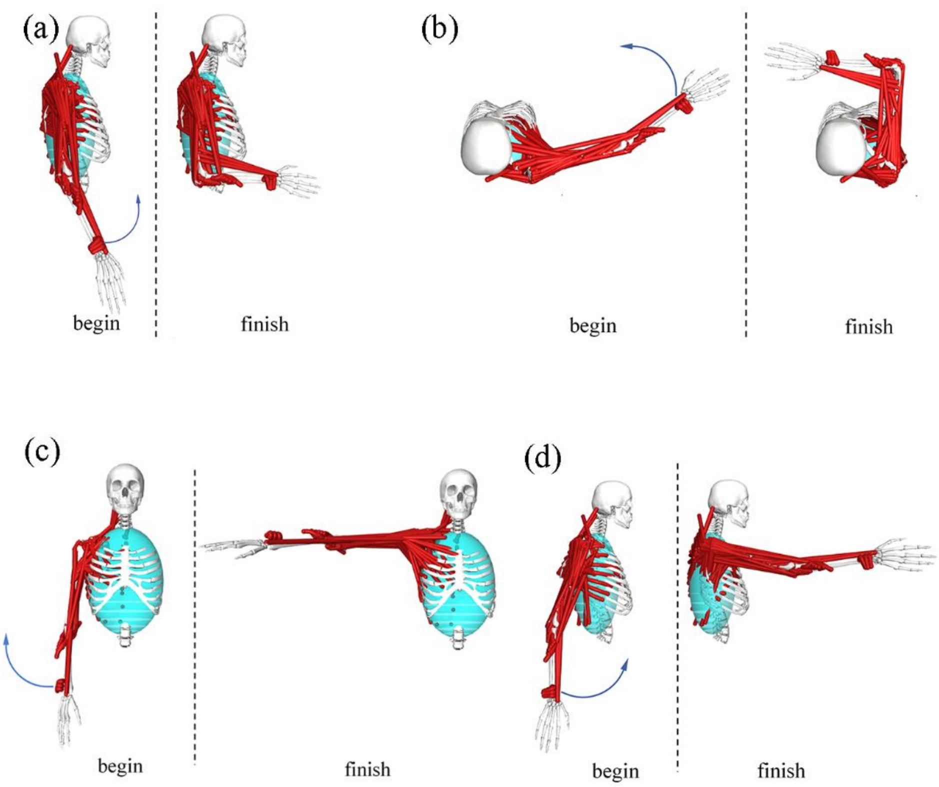

Figure. 1: Simulation analysis of movement process (a) elbow flexion (b) horizontal adduction/abduction (c) vertical abduction/adduction (d) flexion/extension

Table3 Summary of the DAS3 model

Category	Item	Description
General information	Model name	DAS3 (Dynamic Arm Simulator 3)
	Original source	Dynamic arm simulator project
	Primary references	Chadwick et al., 2014
Skeletal structure	Segments	Thorax, clavicle, scapula, humerus, ulna, radius
Joint definition	Shoulder complex	Multi-joint system (SC, AC, GH joints)
	Elbow joint	1 DOF (flexion/extension)
	Forearm joint	1 DOF (pronation/supination)
Musculotendon units	Muscle type	Hill-type muscle model
Applications	Biomechanics	Muscle force estimation, joint load analysis
	Clinical	Rehabilitation assessment
	Engineering	Exoskeleton and prosthesis design

Table 4 Shoulder joint IK

Shoulder joint IK	Elbow flexion movement	Horizontal adduction/abduction movement	vertical abduction/adduction movement	Flexion/extension movement
0-1	0°-0°	0°-18.26°	-30.6°--6.66°	0°-18.42°
1-3	0°-0°	18.26°-54.78°	6.66°-41.22°	18.42°-55.26°
3-5	0°-0°	54.78°-91.3°	41.22°-89.1°	55.26°-92.1°

Table 5 Elbow joint IK

Elbow joint IK	Elbow flexion movement	Horizontal adduction/abduction movement	vertical abduction/adduction movement	Flexion/extension movement
0-1	0°-18.3°	0°-18.7°	0°-0°	0°-0°
1-3	18.3°-54.9°	18.7°-56.1°	0°-0°	0°-0°
3-5	54.9°-91.5°	56.1°-93.5°	0°-0°	0°-0°

ACCEPTED

2.3 Design of the Upper Limb Rehabilitation Mechanisms

Based on the physiological trajectories derived from the OpenSim simulations, two distinct types of upper limb rehabilitation mechanisms—an exoskeleton type and an end-effector type—were designed. Prior to structural modeling, the required degrees of freedom (DOF) for each mechanism were calculated using the general mobility formula:

$$F=3n-2P_L-P_H \tag{1}$$

where F represents the total DOF of the mechanism, n denotes the number of moving links, P_L is the number of lower kinematic pairs, and P_H indicates the number of higher kinematic pairs.

2.3.1 Exoskeleton Mechanism Design

According to the DOF analysis, the exoskeleton mechanism as a whole has 5 passive adjustable degrees of freedom, but the active drive module is simplified to 2 core joint degrees of freedom for analysis. Designed to fully enclose the upper limb and replicate natural human joint kinematics, the mechanism utilizes the upper and forearm parts of the model as driving linkages. The structural configuration comprises three serially connected modules: the shoulder, elbow, and wrist mechanisms (fig. 2).

The shoulder module features a 2-DOF design facilitating for horizontal adduction/abduction and flexion/extension via disc hinge connections. The elbow module provides a single-DOF motion for horizontal adduction/abduction, ensuring alignment between the mechanical hinges and the anatomical rotation axes. Adjustable link lengths and strap systems were incorporated to accommodate diverse anthropometric dimensions and minimize misalignment-induced stress.

ACCEPTED

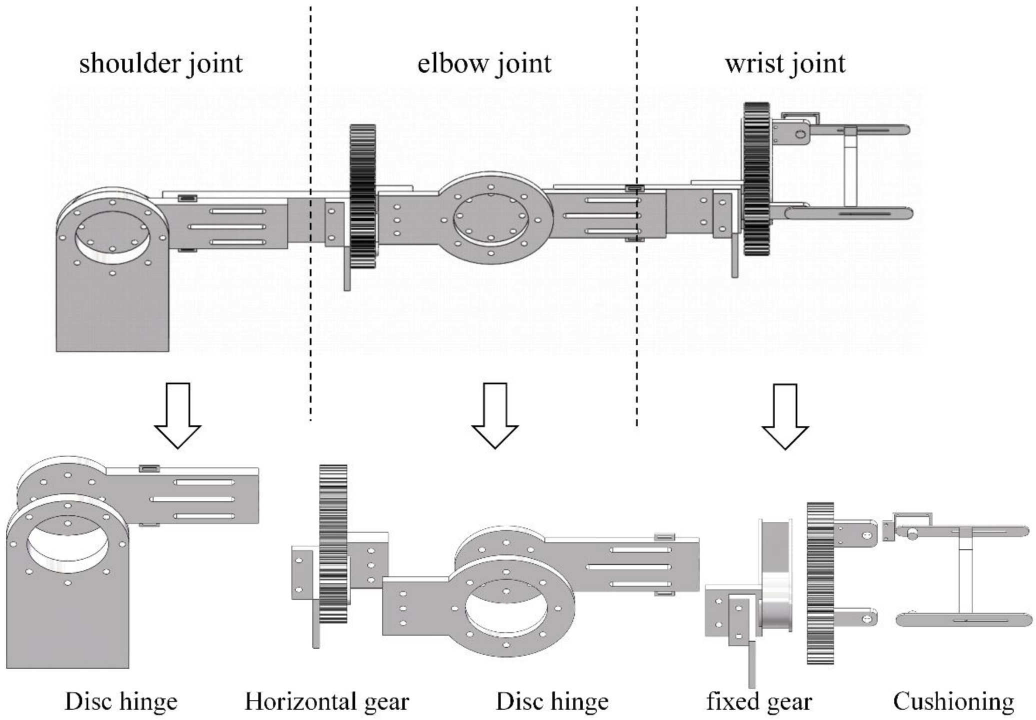

Figure. 2: Exoskeleton mechanism

2.3.2 End-Effector Mechanism Design

Conversely, the end-effector mechanism was conceptualized as a 3-DOF linkage system containing two lower pairs and two higher pairs. Unlike the exoskeleton, this mechanism operates in series with the biological limb, applying traction forces to the distal end (hand/wrist) to drive the proximal joints.

The system is composed of a multi-segment serial robotic arm, a traction device, and a terminal effector (fig. 3). The robotic arm utilizes revolute joints to achieve the necessary horizontal and oblique spatial displacements required for horizontal adduction/abduction and flexion/extension exercises. The terminal effector features a customized glove-type interface that secures the hand and transmits directional pulling forces via cables or steel bands, without directly constraining the intermediate elbow or shoulder joints.

ACCEPTED

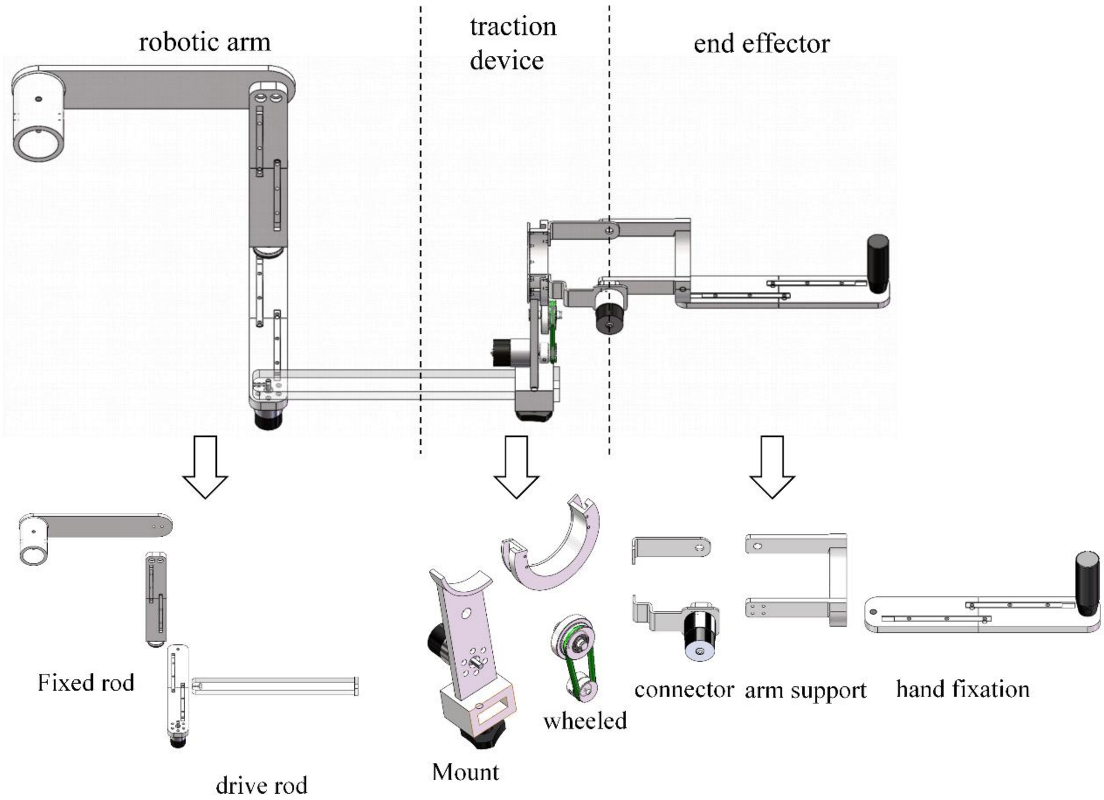

Figure. 3: End-effector mechanism

2.4 Co-Simulation and Performance Evaluation Protocol

To comparatively evaluate the trajectory adaptability and biomechanical safety of the two designed mechanisms, virtual prototype co-simulations and R^2 calculation were conducted. Before using ADAMS for simulation analysis, import the two mechanism models into the software for parameter settings. Set the link length to static, set the model to aluminum alloy material in the software, and add fixed and rotating pairs.

2.4.1 Trajectory Similarity Analysis

The 3D models of both mechanisms were imported into ADAMS 2020 (Automatic Dynamic Analysis of Mechanical Systems) software, adjusting the model coordinate system. To ensure cross platform consistency, all models are defined in a unified global coordinate system (right-handed Cartesian system, with the origin at the shoulder joint center). Using the inverse kinematics data generated in OpenSim (tables 4 and 5) as a reference, input the rotational pairs and mechanism drives of two mechanisms in

ADAMS to simulate the continuous motion of rehabilitation tasks. Set the center point of the mechanism end as the trajectory sampling point to obtain the motion trajectory of the mechanism. The spatial coordinates of the end-effectors were extracted from ADAMS and imported into MATLAB R2022b. To quantify the kinematic fidelity of the devices, the discrete Fréchet distance algorithm was employed to calculate the geometric similarity between the device-generated trajectories and the ideal human physiological trajectories. A smaller Fréchet distance indicates higher trajectory precision.

2.4.2 Analysis of Trajectory Determination Coefficient

To quantitatively evaluate the trajectory tracking performance of different rehabilitation mechanisms, Evaluate the similarity between the mechanism trajectory and human model trajectory through the coefficient of determination (R^2). Sample and align the trajectory data of the human body model and the trajectory data of the two mechanisms in a unified coordinate system according to time (tables 6 and 7) and calculate the R^2 of the trajectories of the two mechanisms. R^2 calculation formula:

$$R^2 = 1 - \frac{\sum_{i=1}^{n}(y_i - \hat{y}_i)^2}{\sum_{i=1}^{n}(y_i - \bar{y}_i)^2} \tag{2}$$

where R^2 represents the coefficient of determination of the mechanism, y_i is the trajectory value of the human body model, $\hat{y}$ is the trajectory value of the mechanism, and $\bar{y}$ is the mean trajectory value of the human body model.

Table 6 Horizontal adduction/abduction trajectory data

Time	Human X	Human Y	Exo X	Exo Y	End X	End Y
0	0.5500	0.0000	0.5497	0.0174	0.5470	-0.0519
0.25	0.5499	0.0088	0.5493	0.0267	0.5487	-0.0335
0.5	0.5488	0.0348	0.5479	0.0459	0.5499	0.0073
0.75	0.5439	0.0771	0.5438	0.0778	0.5459	0.0650
1	0.5315	0.1335	0.5343	0.1231	0.5338	0.1267
1.25	0.5070	0.2006	0.5133	0.1861	0.5112	0.1928
1.5	0.4669	0.2728	0.4739	0.2620	0.4785	0.2564
1.75	0.4089	0.3431	0.4099	0.3422	0.4324	0.3197
2	0.3341	0.4042	0.3229	0.4113	0.3639	0.3848
2.25	0.2462	0.4492	0.2220	0.4578	0.2684	0.4421
2.5	0.1516	0.4740	0.1184	0.4777	0.1482	0.4769

ACCEPTED

2.75	0.0580	0.4776	0.0240	0.4739	0.0212	0.4763
3	-0.0275	0.4625	-0.0528	0.4544	-0.0844	0.4450
3.25	-0.0999	0.4337	-0.1105	0.4280	-0.1563	0.4026
3.5	-0.1569	0.3975	-0.1546	0.3992	-0.1974	0.3668
3.75	-0.1984	0.3602	-0.1905	0.3682	-0.2185	0.3434
4	-0.2265	0.3268	-0.2183	0.3373	-0.2321	0.3256
4.25	-0.2439	0.3008	-0.2373	0.3111	-0.2404	0.3133
4.5	-0.2531	0.2845	-0.2484	0.2930	-0.2435	0.3085
4.75	-0.2559	0.2790	-0.2527	0.2851	-0.2409	0.3124
5	-0.2600	0.2751	-0.2517	0.2844	-0.2379	0.3129

Table 7 Flexion/extension trajectory data

Time	Human X	Human Y	Exo X	Exo Y	End X	End Y
0	-0.2800	-0.4734	-0.2648	-0.4820	-0.3173	-0.4490
0.25	-0.2732	-0.4773	-0.2574	-0.4860	-0.3027	-0.4590
0.5	-0.2527	-0.4885	-0.2428	-0.4935	-0.2703	-0.4789
0.75	-0.2183	-0.5048	-0.2176	-0.5051	-0.2226	-0.5029
1	-0.1698	-0.5231	-0.1801	-0.5197	-0.1696	-0.5232
1.25	-0.1076	-0.5394	-0.1232	-0.5360	-0.1090	-0.5391
1.5	-0.0334	-0.5490	-0.0465	-0.5480	-0.0462	-0.5480
1.75	0.0499	-0.5477	0.0485	-0.5479	0.0235	-0.5494
2	0.1382	-0.5323	0.1517	-0.5287	0.1096	-0.5389
2.25	0.2264	-0.5012	0.2512	-0.4892	0.2107	-0.5080
2.5	0.3091	-0.4549	0.3388	-0.4330	0.3189	-0.4481
2.75	0.3817	-0.3960	0.4087	-0.3678	0.4157	-0.3597
3	0.4409	-0.3288	0.4589	-0.3031	0.4827	-0.2623
3.25	0.4856	-0.2583	0.4922	-0.2453	0.5196	-0.1777
3.5	0.5161	-0.1900	0.5149	-0.1933	0.5363	-0.1195
3.75	0.5348	-0.1286	0.5311	-0.1428	0.5429	-0.0866
4	0.5445	-0.0776	0.5417	-0.0953	0.5463	-0.0633
4.25	0.5486	-0.0397	0.5471	-0.0564	0.5479	-0.0479
4.5	0.5498	-0.0165	0.5492	-0.0300	0.5483	-0.0428
4.75	0.5499	-0.0086	0.5497	-0.0184	0.5475	-0.0501
5	0.5501	-0.0089	0.5504	-0.0094	0.5575	-0.0511

ACCEPTED

2.4.3 Joint Torque Evaluation

To assess biomechanical safety, Using ADAMS dynamic simulation to monitor the rotational torque on the shoulder, elbow, and wrist joints of two mechanisms during the execution of selected rehabilitation exercises. Excessive joint torque concentrations at specific anatomical nodes were established as the primary indicator of potential secondary injury risk during passive training. According to clinical studies on the risk of shoulder subluxation in stroke patients with soft paralysis [7, 10], the maximum safe range of joint torque for rehabilitation training is 30% -50% of the average maximum isometric contraction torque of adult upper limb joints. In this study, the median value of 40Nm was taken as the preliminary safety threshold for joint torque in upper limb rehabilitation training.

ACCEPTED

3. Results

3.1 Kinematic Analysis and Selection of Rehabilitation Movements

Initial kinematic measurements of the six fundamental passive upper limb rehabilitation movements are summarized in table 2. Analysis of the average ROM across five trials revealed that the rotational amplitudes for shoulder internal/external rotation and elbow internal/external rotation were small. Consequently, these two movements were excluded from further biomechanical evaluation.

The remaining four movements (elbow flexion, horizontal adduction/abduction, vertical abduction/adduction, flexion/extension) were simulated in OpenSim to analyze dynamic muscle force variations. As illustrated in fig. 4, the forearm (red lines) and upper arm (black lines) muscle groups exhibited distinct activation patterns across the different exercises.

During elbow flexion (fig. 4a), the forearm muscle force showed significant variation, peaking at 39.23 N (at 5 s, with a flexion angle of 91.5°), while the upper arm force remained relatively stable at approximately 12.4 N. In horizontal adduction/abduction (fig. 4b), both forearm and upper arm muscles exhibited notable synchronous engagement, peaking at 20.16 N (28.9°) and 56.68 N (36.8°), respectively, and stabilizing around 18.86 N and 55.74 N during the maintenance phase. In vertical abduction/adduction (fig. 4c), upper arm force peaked sharply at 59.98 N, but forearm activation was negligible (0.7 N). In flexion/extension (fig. 4d), the upper arm muscle force varied significantly, reaching a peak of 61.32 N (89.1°), with the forearm force remaining constant near 10 N. Conversely.

Perform muscle force data sampling on the movement process of four actions, screen for actions with high muscle force activation through RMS analysis. The formula for calculating RMS is:

$$RMS = \sqrt{\frac{1}{n}\sum_{i=1}^{n} x_i^2} \tag{3}$$

Collectively, based on the muscle force data calculated by the formula (table 8), the involvement of the upper arm is relatively high in horizontal adduction/abduction,

ACCEPTED

vertical abduction/adduction and flexion/extension. Elbow flexion shows significant forearm activation but incomplete upper arm training. To ensure full participation and structural verification of the upper limbs, selecte horizontal adduction/abduction and flexion/extension as the target guidance trajectories for the mechanism simulation. The selected action space trajectory generated through OpenSim is shown in fig. 5.

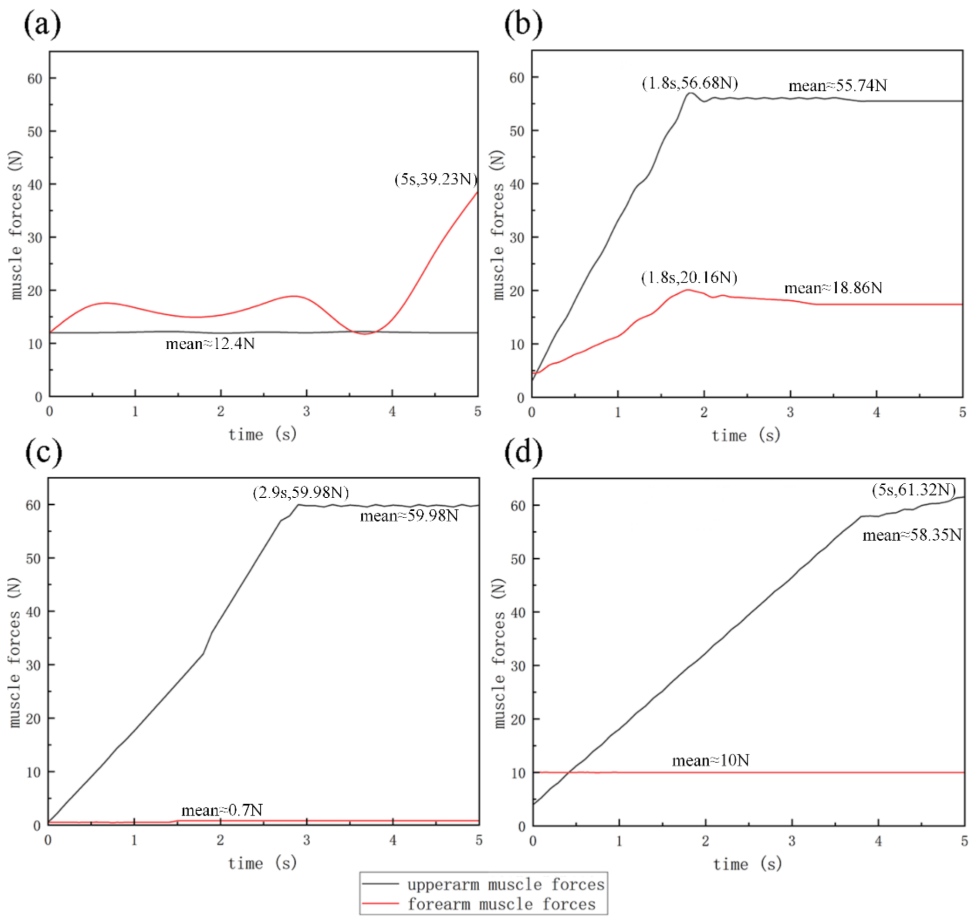

Figure. 4: Changes in upper limb muscle force (a) elbow flexion (b) horizontal adduction/abduction (c) vertical abduction/adduction (d) flexion/extension

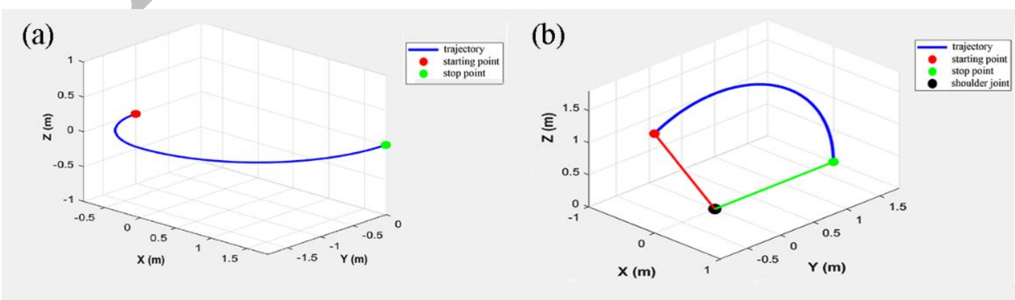

Figure. 5: Upper limb model motion trajectory (a) horizontal adduction/abduction trajectory (b) flexion/extension trajectory

Table 8 Muscle strength RMS data

time(s)	elbow flexion		horizontal adduction/abduction		vertical abduction/adduction		flexion/extension	
	upper(N)	fount(N)	upper(N)	fount(N)	upper(N)	fount(N)	upper(N)	fount(N)
0	12.40	12.40	4.26	4.13	6.00	0.49	7.00	10.00
0.25	12.45	13.50	11.18	6.27	6.00	0.65	7.00	10.05
0.5	12.35	16.80	18.10	8.41	8.50	0.75	9.50	9.95
0.75	12.48	16.70	25.02	10.55	12.50	0.68	13.20	10.08
1	12.32	15.70	31.94	12.69	17.50	0.72	18.50	9.92
1.25	12.43	15.11	38.86	14.83	18.50	0.63	19.20	10.03
1.5	12.37	14.50	45.78	16.97	27.40	0.75	28.50	9.97
1.75	12.41	13.40	55.20	19.80	28.50	0.69	29.80	10.01
2	12.39	14.41	55.74	18.80	37.50	0.71	39.80	9.99
2.25	12.46	16.19	55.76	18.61	39.20	0.66	41.50	10.06
2.5	12.34	18.53	55.73	18.34	47.80	0.74	50.80	9.94
2.75	12.44	20.21	55.74	18.20	53.10	0.67	52.60	10.02
3	12.36	18.50	55.75	18.20	59.40	0.73	54.40	9.98
3.25	12.42	16.80	55.77	18.17	59.30	0.64	56.20	10.04
3.5	12.38	15.10	55.74	18.15	59.50	0.76	58.00	9.96
3.75	12.40	12.60	55.73	18.14	59.60	0.70	58.40	10.07
4	12.41	15.80	55.52	18.11	59.70	0.70	59.60	9.93
4.25	12.39	19.82	55.71	18.09	59.80	0.68	59.70	10.00
4.5	12.40	27.35	55.78	18.04	59.80	0.72	60.20	10.00
4.75	12.40	34.18	55.76	18.01	59.70	0.69	61.50	10.00
5	12.40	39.23	55.72	18.01	59.70	0.71	62.40	10.00
RMS	12.401	19.200	45.997	15.848	42.840	0.691	42.727	10.010

3.2 Motion Trajectory Simulation and Similarity Analysis

Based on the mechanism design principles (exoskeleton confirmed as 2-DOF and end-effector as 3-DOF linkage systems, as detailed in table 9), the virtual prototypes were driven in ADAMS. Both mechanisms successfully completed the assigned rehabilitation motions without kinematic singularities (fig. 6).

The kinematic fidelity of the mechanisms was quantified using discrete Fréchet distance analysis in MATLAB, comparing the device-generated trajectories with the

ACCEPTED

natural physiological trajectories (fig. 7).

The simulation results demonstrated a significant discrepancy in trajectory precision between the two device types. For the end-effector mechanism, the Fréchet distance was calculated as 5 mm during flexion/extension (fig. 7a) and 3 mm during horizontal adduction/abduction (fig. 7b). In contrast, for the exoskeleton mechanism, the Fréchet distance was calculated as 2 mm during flexion/extension (fig. 7c) and 1 mm during horizontal adduction/abduction (fig. 7d). The data indicates that the exoskeleton-type device achieves extremely high similarity to natural human motion (errors controlled within ≤ 2 mm) due to independent joint alignment, whereas the end-effector device exhibits a comparatively weaker fit (errors controlled within ≤ 5 mm).

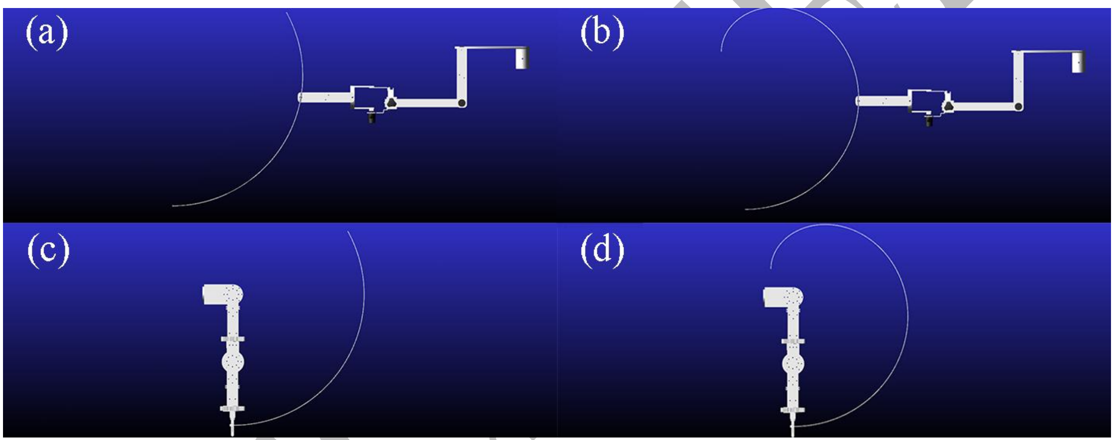

Figure. 6: End of mechanism trajectories (a) end-effector during flexion/extension (b) end-effector trajectory during adduction/abduction (c) exoskeleton-type during flexion/extension (d) exoskeleton during horizontal adduction/abduction.

ACCEPTED

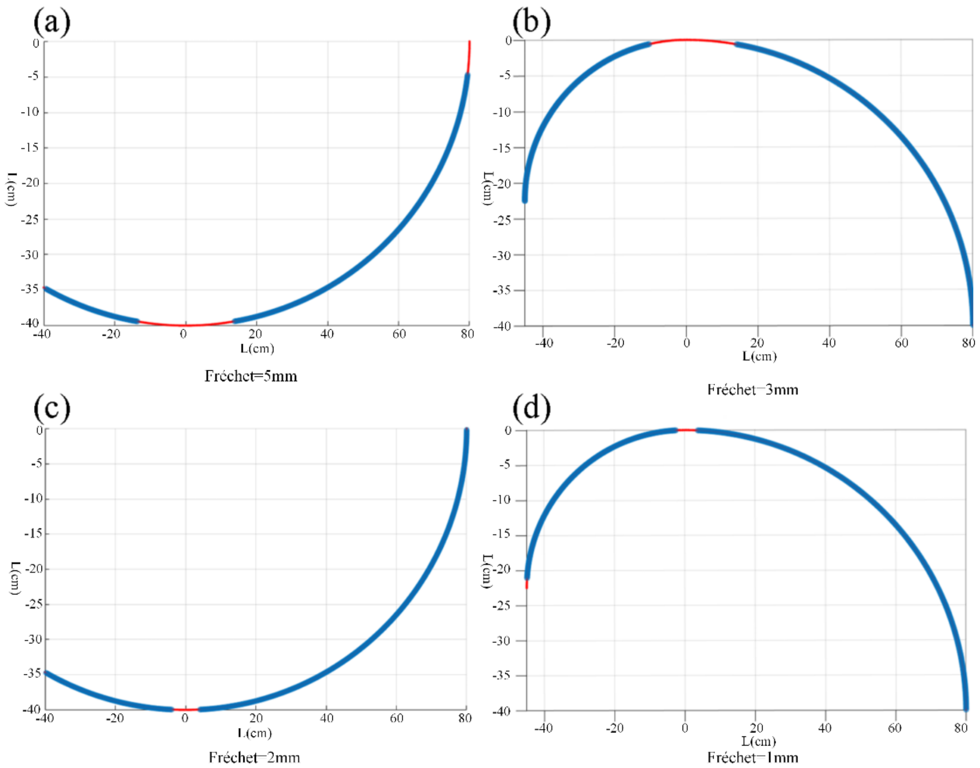

Figure. 7: Trajectory fitting (a) end-effector during flexion/extension (b) end-effector during horizontal adduction/abduction (c) exoskeleton during flexion/extension (d) exoskeleton during horizontal adduction/abduction.

Table 9 Number of mechanism components

Mechanism type	Movable links in Mechanism(n)	Lower pairs(PL)	Higher pairs(PH)	Degrees of freedom(F)
Exoskeleton	2	2	0	2
End-effector	3	2	2	2

3.3 Calculation and Analysis of Trajectory Determination Coefficient

R^2 is used to quantify the similarity between the trajectory of the mechanism and the reference human motion trajectory. R^2 value close to 1 indicates a higher degree of trajectory matching. Substitute the trajectory data (tables 6 and 7) into the determination coefficient formula (eq. (2)) for calculation.

According to the formula, the R^2 values of the end-effector mechanism in two movements are 0.9942 and 0.9910, respectively, while the R^2 values of the exoskeleton mechanism in two movements are 0.9988 and 0.9975, respectively. The overall trajectory difference in fig. 8.

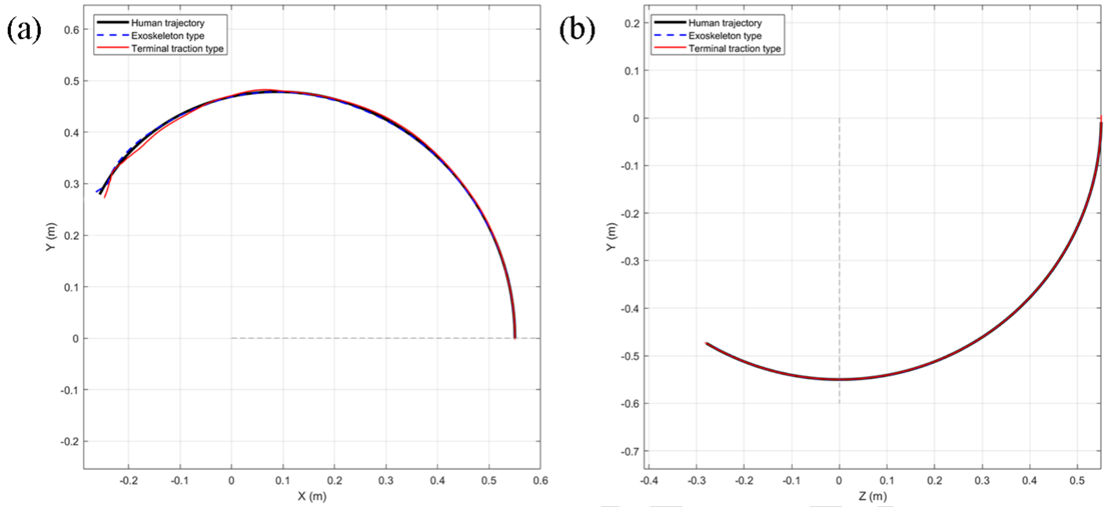

Figure. 8: Comparison of R2 data trajectories at the end of mechanisms (a) horizontal adduction/abduction comparison (b) flexion/extension comparison

3.4 Joint Torque Evaluation and Biomechanical Safety

The dynamic rotational torques experienced by the upper limb joints during the execution of the rehabilitation trajectories are presented in fig. 9.

During both flexion/extension and horizontal adduction/abduction, Simulation results for the end-effector mechanism (fig. 9a and 9b) revealed significant stress concentrations at the distal joints, the joint moments for the wrist and elbow exhibited sharp fluctuations, > 40 Nm at their peaks. Although the overall moment changes were relatively modest during horizontal movements, the wrist joint torque still > 40 Nm, and the shoulder joint approached this limit.

Conversely, the exoskeleton mechanism demonstrated a highly balanced torque distribution (fig. 9c and 9d). During flexion/extension, all joint torque variations remained strictly < 40 Nm. Similarly, throughout the entire movement cycle of horizontal adduction/abduction, the joint moment fluctuations for the shoulder, elbow, and wrist stayed consistently < 30 Nm. These findings quantitatively confirm that the exoskeleton design significantly reduces abnormal joint loading compared to the end-effector approach.

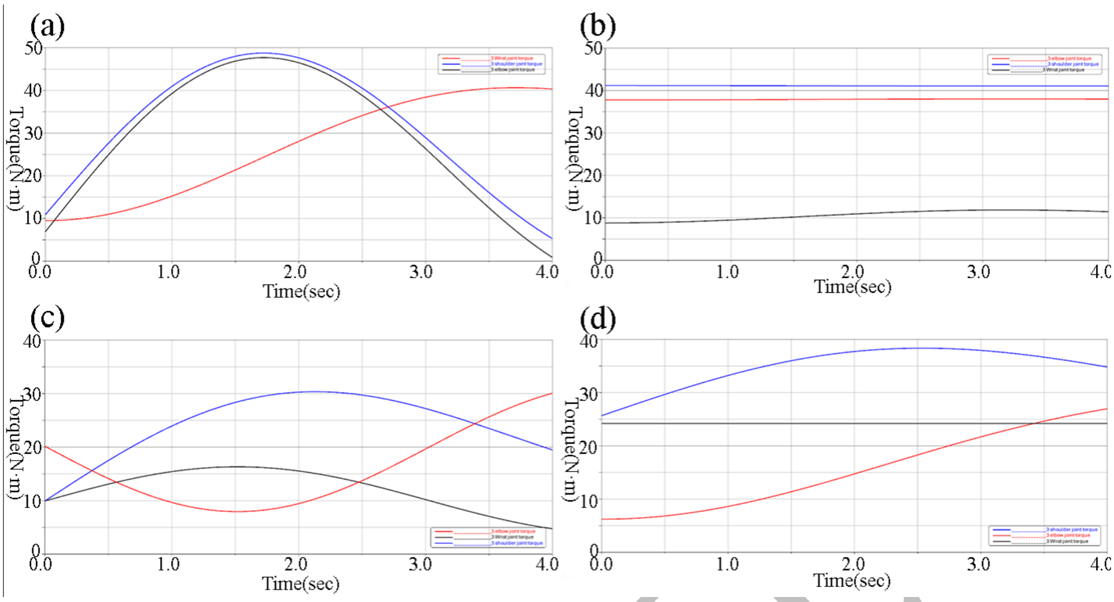

Figure. 9: Variation of joint torque (a) flexion/extension with end-effector mechanism (b) horizontal adduction/abduction with end-effector mechanism (c) flexion/extension with exoskeleton mechanisms (d) horizontal adduction/abduction with exoskeleton mechanisms

4. Discussion

The primary objective of this study was to compare the kinematic trajectory adaptability and biomechanical safety (joint torque variations) of two mainstream upper limb rehabilitation mechanisms—exoskeleton and end-effector types—during passive training. By integrating musculoskeletal modeling with dynamic mechanical simulation, we quantitatively evaluated both devices under identical physiological movement conditions.

4.1 Kinematic Fidelity and Structural Mechanisms

Our trajectory similarity analysis utilizing the discrete Fréchet distance revealed that the exoskeleton mechanism significantly outperformed the end-effector mechanism (errors ≤ 2 mm vs. ≤ 5 mm). This discrepancy fundamentally stems from their structural paradigms. The exoskeleton is designed with joint axis alignment, meaning its mechanical hinges physically coincide with the patient’s anatomical rotation centers. This configuration allows for precise, independent control of

ACCEPTE

individual joint angles, effectively replicating complex three-dimensional human motions.

Conversely, the end-effector mechanism operates by constraining only the distal extremity (the hand or wrist) and relies on inverse kinematics to drive the entire upper limb. Because it lacks direct control over the intermediate joints (elbow and shoulder), spatial deviations are inevitable when simulating multi-joint coordinated movements, leading to a lower fit to natural physiological patterns.

In coefficient of determination analysis, exoskeleton-type trajectory $R^2 \geq 0.9975$ better than end-effector-type trajectory $R^2 \geq 0.9910$. Prove that exoskeleton mechanisms are superior to end effector mechanisms in trajectory fitting.

4.2 Biomechanical Safety and Clinical Implications

A critical finding of this study is the drastic difference in joint torque distribution between the two mechanisms. During passive rehabilitation exercises, the end-effector device generated excessive torques ($>$ 40 Nm) at the wrist and elbow joints. From a biomechanical perspective, applying a driving force at the terminal end creates a significant lever-arm effect. To overcome the inertia and gravity of the entire arm, the distal actuator must exert substantial force, which translates into concentrated stress at the proximal joints.

For patients in the early flaccid stage of stroke recovery (Brunnstrom Stage I), muscle tone is virtually absent, and the ligaments are highly vulnerable. Subjecting these patients to concentrated torques $>$ 40 Nm poses a severe risk of secondary injuries, such as shoulder subluxation or ligament sprains. Therefore, our results strongly suggest that end-effector systems require highly advanced force-compliance algorithms (e.g., impedance/admittance control) to mitigate biomechanical risks, as traditional rigid position control is unsafe for early-stage passive training.

In contrast, the exoskeleton mechanism maintained balanced joint moments strictly between 30-40 Nm throughout all movement cycles. By applying distributed forces locally at each corresponding joint, the exoskeleton eliminates the long lever-arm effect. This makes the exoskeleton intrinsically safer and highly suitable for passive

ACCEPTED

motion assistance and ROM recovery in early-stage stroke rehabilitation. However, it is worth noting that while exoskeletons offer superior joint protection, they demand precise donning procedures; any misalignment between the mechanical and anatomical axes during practical application could introduce parasitic forces, necessitating adjustable and compliant coupling designs.

4.3 Limitations and Future Work

Despite the comprehensive framework proposed in this study, several limitations should be acknowledged.

Trajectory similarity does not necessarily reflect actual limb motion during human–robot interaction, as relative displacement may occur due to soft tissue deformation, compliance, and alignment errors, potentially leading to overestimated performance. The current model does not fully represent the complexity of the shoulder complex. The dynamic motion of the shoulder joint center and simplified modeling assumptions may introduce kinematic incompatibility and increased interaction forces. Human–robot interface mismatch remains a challenge. Although adjustable mechanisms are included, precise alignment is difficult to achieve due to anatomical variability, resulting in unavoidable trade-offs that were not fully quantified.

Results are based on simulations without experimental validation. Key real-world factors, such as actuator dynamics, control delays, and user adaptation, were not considered, limiting clinical applicability.

Future work will address these limitations by developing subject-specific and compliant human–robot interaction models, incorporating detailed shoulder complex kinematics, and improving interface design for better alignment and adaptability. Moreover, physical prototypes will be constructed and validated through experimental studies involving both healthy participants and stroke patients, using techniques such as motion capture, surface electromyography (sEMG), and force/torque sensing. These efforts will enable a more realistic assessment of device performance and support the translation of simulation findings into clinical applications.

ACCEPTED

5. Conclusion

This study systematically compared the kinematic trajectory adaptability and biomechanical safety of exoskeleton-type and end-effector-type upper limb rehabilitation mechanisms through musculoskeletal and dynamic co-simulations. Initial biomechanical analysis using OpenSim identified horizontal adduction-abduction and anterior-posterior flexion as the most effective passive exercises for comprehensive upper limb muscle engagement during the flaccid stage of stroke recovery, establishing them as optimal guiding trajectories for subsequent mechanism design.

Comparative simulations demonstrated that the exoskeleton mechanism achieves significantly higher fidelity in replicating natural human arm trajectories, with discrete Fréchet distance errors $\leq$ 2 mm. In contrast, the end-effector system exhibited a lower fit to physiological movement patterns, showing tracking errors $\leq$ 5 mm. In coefficient of determination analysis, exoskeleton-type trajectory $R^2 \geq 0.9975$ better than end-effector-type trajectory R2 $\geq$ 0.9910. Furthermore, dynamic joint torque evaluations revealed that the exoskeleton device effectively maintains balanced rotational moments across the shoulder, elbow, and wrist joints, keeping them well $<$ 40 Nm. Conversely, the end-effector design generates concentrated lever-arm forces that result in excessive torques at the distal joints, posing potential stress injury risks during passive training.

Ultimately, exoskeleton-type mechanisms exhibit clear advantages in both trajectory precision and joint protection, making them highly suitable for passive motion assistance and range-of-motion recovery in early-stage rehabilitation. While end-effector systems offer structural simplicity and spatial flexibility for complex motions, their safe application necessitates the integration of advanced force-compliance algorithms to mitigate concentrated terminal forces and ensure biomechanical safety.

ACCEPTED

Statements and Declarations

Competing Interests:

The authors declare that they have no known competing financial interests or personal relationships that could have appeared to influence the work reported in this paper. The authors confirm that this manuscript has not been published previously and is not currently under consideration for publication elsewhere.

Finding:

This research did not receive any specific grant from funding agencies in the public, commercial, or not-for-profit sectors.

Credit Authorship Contribution Statement:

Haoyu Han: Writing – original draft

Li Feng: Writing – review & editing

Qinghui Zhu: Software

Data Availability Statement:

The datasets supporting this study are available from the corresponding author upon reasonable request.

ACCEPTED

References

1. Babaiasl, M., Mahdioun, S. H., Jaryani, P., and Yazdani, M. (2016) A review of technological and clinical aspects of robot-aided rehabilitation of upper-extremity after stroke Disabil Rehabil Assist Technol 11, 263-280. doi:10.3109/17483107.2014.1002539
2. Cao, Q., Li, L., Li, J., Li, R., and Wang, X. (2025) A methodology to quantify human-robot interaction forces: a case study of a 4-DOFs upper extremity rehabilitation robot Robotica 43, 1469-1490
3. Cheng, H., Huang, R., Qiu, J., Wang, Y., Zou, C., and Shi, K. (2021) A Survey of Rehabilitation Robot and Its Clinical Applications Jiqiren/Robot 43, 606-619
4. Feigin, V. L., Forouzanfar, M. H., Krishnamurthi, R., Mensah, G. A., Connor, M., Bennett, D. A. et al. (2014) Global and regional burden of stroke during 1990-2010: findings from the Global Burden of Disease Study 2010 Lancet 383, 245-254. doi:10.1016/S0140-6736(13)61953-4
5. Fernández-Valdés, B. (2021) Movement variability in resistance training in team sports,
6. Flynn, N., Froude, E., Cooke, D., Dennis, J., and Kuys, S. (2022) The sustainability of upper limb robotic therapy for stroke survivors in an inpatient rehabilitation setting Disabil Rehabil 44, 7522-7527. doi:10.1080/09638288.2021.1955307
7. Holzbaur, K. R. S., Murray, W. M., & Delp, S. L. (2005). A model of the upper extremity for simulating musculoskeletal surgery and analyzing neuromuscular control. Annals of Biomedical Engineering, 33(6), 829-840. doi:10.1007/s10439-005-3320-7
8. Hsu, H. Y., Yang, K. C., Yeh, C. H., Lin, Y. C., Lin, K. R., Su, F. C. et al. (2022) A Tenodesis-Induced-Grip exoskeleton robot (TIGER) for assisting upper extremity functions in stroke patients: a randomized control study Disabil Rehabil 44, 7078-7086. doi:10.1080/09638288.2021.1955306
9. Hynčík, L., Čechová, H., Bońkowski, T., Kavalířová, G., Špottová, P., Hampejsová, V. et al. (2021) Personalization of a Human Body Model Using Subject-Specific Dimensions for Designing Clothing Patterns Applied Sciences 11, 10138. doi:10.3390/app112110138
10. Lambercy, O., Dovat, L., Gassert, R., Burdet, E., Teo, C. L., & Milner, T. (2007). A haptic knob for rehabilitation of hand function. Ieee Transactions on Neural Systems and Rehabilitation Engineering, 15(3), 356-366. doi:10.1109/tnsre.2007.903913
11. Langerak, A. J., D'Olivo, P., Thijm, O. S. A., Regterschot, G. R. H., Meskers, C. G. M., Rozendaal, M. C. et al. (2024) Stroke patients' motivation for home-based upper extremity rehabilitation with eHealth tools Disabil Rehabil 46, 5323-5333. doi:10.1080/09638288.2023.2245963
12. NIKOOYAN A A, VEEGER H E J, WESTERHOFF P, et al. Validation of the shoulder network model of the Delft Shoulder and Elbow Model (DSEM)[J]. Medical & Biological Engineering & Computing, 2011, 49(12): 1425-1435.
13. NIKOOYAN A A, VEEGER H E J, VAN DER HELM F C T, et al. A

ACCEPTED

musculoskeletal model of the upper extremity for simulating muscle forces and joint contact forces[J]. Biological Cybernetics, 2012, 106(3): 189-204.

14. Persson, H. C., Parziali, M., Danielsson, A., and Sunnerhagen, K. S. (2012) Outcome and upper extremity function within 72 hours after first occasion of stroke in an unselected population at a stroke unit. A part of the SALGOT study BMC Neurol 12, 162. doi:10.1186/1471-2377-12-162
15. Sun, J., Foroutani, Y., and Rosen, J. (2025) Virtually Constrained Admittance Control Using Feedback Linearization for Physical Human-Robot Interaction With Rehabilitation Exoskeletons IEEE/ASME Transactions on Mechatronics 30, 898-909. doi:10.1109/TMECH.2024.3351234
16. Sun, J., Kramer, E. H., and Rosen, J. (2025) A Safety-Focused Admittance Control Approach for Physical Human–Robot Interaction With Rigid Multi-Arm Serial Link Exoskeletons IEEE/ASME Transactions on Mechatronics 30, 414-425. doi:10.1109/TMECH.2024.3345678
17. Wang, Y., Peng, Q., Guo, J., Zhou, L., and Lu, W. (2020) Age-Period-Cohort Analysis of Type-Specific Stroke Morbidity and Mortality in China Circ J 84, 662-669. doi:10.1253/circj. CJ-19-0903
18. Yang, S., Boudier-Revéret, M., Kwon, S., Lee, M. Y., and Chang, M. C. (2021) Effect of Diabetes on Post-stroke Recovery: A Systematic Narrative Review Front Neurol 12, 747878. doi:10.3389/fneur.2021.747878
19. Zhang, X., Zheng, Z., and Qi, Y. (2016) Parameter identification and calibration of D-H model for 6-DOF serial robots 38, 360-370

ACCEPTED